Supplementary Information

Enhanced Fluorescence of [[5'-(4-hydroxyphenyl) [2,2'-bithiophen]-5-yl]methylene]-propanedinitrile (NIAD-4): Solvation Induced Micro-Viscosity Enhancement

Jiangpu Hu, Huaning Zhu, Yang Li, Xian Wang, Renjun Ma, Qianjin Guo*, Andong Xia*

Beijing National Laboratory for Molecular Sciences (BNLMS), The Key Laboratory of Photochemistry, Institute of Chemistry, Chinese Academy of Sciences, Beijing 100190, People's Republic of China

* Corresponding author: andong@iccas.ac.cn; guoqj@iccas.ac.cn

Contents

S1. Orbital and charge property

Figure S1 shows the highest occupied molecular orbital (HOMO) and lowest unoccupied molecular orbital (LUMO) and the charge different density (CDD) image of NIAD-4. It is found that the optical HOMO-LUMO transition should have a charge-transfer nature with the electron density shifting mostly from the electron-donating hydroxyphenyl moiety to the accepting dicyanomethylene moiety. In the CDD image between S_1 and S_0 we can see that all holes (blue color) and charges (red color) are fully seperated, also suggesting the ICT nature of NIAD-4.
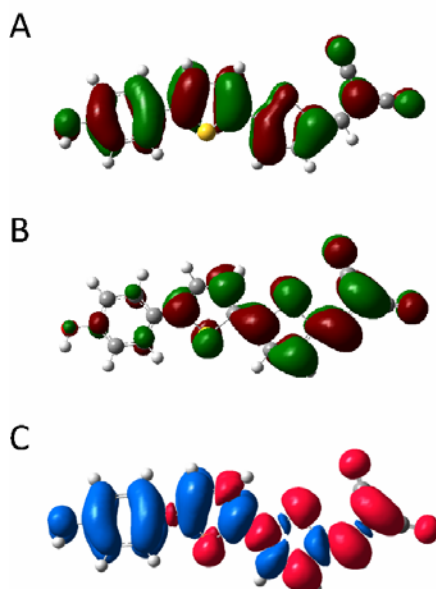

Figure S1. HOMO (A) LUMO (B) and CDD image (C) of NIAD-4.

S2. Dependence of fluorescence quantum yield and viscosity in aprotic solvents

Figure S2 shows the dependence $\Phi/(1-\Phi)$ vs (η/T) for NIAD-4 in aprotic solvents at 293 K. It can be found that the fluorescence quantum yields of NIAD-4 in aprotic solvents don't exhibit linerly dependence relationship as we tested in the alcoholic solvents.
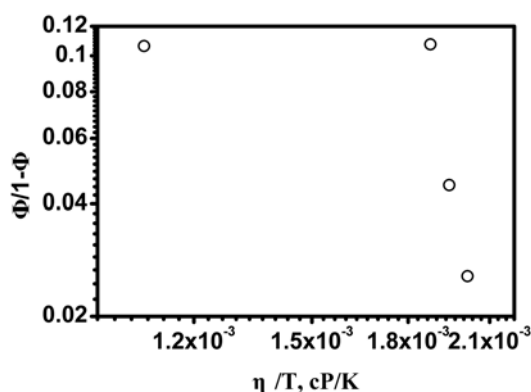

Figure S2. Dependence $\Phi/(1-\Phi)$ vs (η/T) for NIAD-4 in aprotic solvents at 293 K

S3. Femtosecond transient absorption results in alcoholic solvents

Figure S3 depicts the transient absorption spectra for NIAD-4 in methanol and *n*-butanol. It is observed that the initial transient absorption spectra (0.7 ps) in both solvents are comprised by a very broad positive excited-state absorption (ESA) band ranging from about 570 to 660 nm and two negative transient absorption bands located around 470 nm and 690 nm, which can be assigned to ground state bleach (GSB) and simulated emission (SE), respectively, by comparing with the steady state absorption and fluorescence spectra. SE bands ranging from 620 to 740 nm are found in alcoholic solvents, which is attributed to the large bathochromic shift of SE with the increasing of solvent polarity from aprotic solvents to alcoholic solvents on the basis of the steady state fluorescence spectra, leading to the formation of ICT' state. In according to the analysis in aprotic solvents, the rise of new ESA band peaked at around 540 nm is assigned to the formation of TICT state. Isosbestic point is found in both solvents suggesting the torsion of NIAD-4 from ICT' state to TICT state. In addition, the remarkable blue shift of ESA peak of ICT from 640 nm to 620 nm also indicates the strong solvation in alcoholic solvents with high polarities. However the time region of the torsional motion in methanol is only about 6 ps, which is much shorter than that in *n*-butanol (60 ps), indicating that the twisting of NIAD-4 is severely restricted by the high macro-viscosity solvent. The representative evolution associated difference spectra (EADS) and concentration kinetics for NIAD-4 in these alcoholic solvents are extracted and plotted in Figure S4, through globe fitting analysis. It is noted that the torsion time constant is 30.6 ps in *n*-butanol which is much larger than that in methanol suggesting the severely restriction of NIAD-4 in high viscosity solvents. Meanwhile, the both decay process of ICT and TICT state were slowed down by high macro-viscosity.
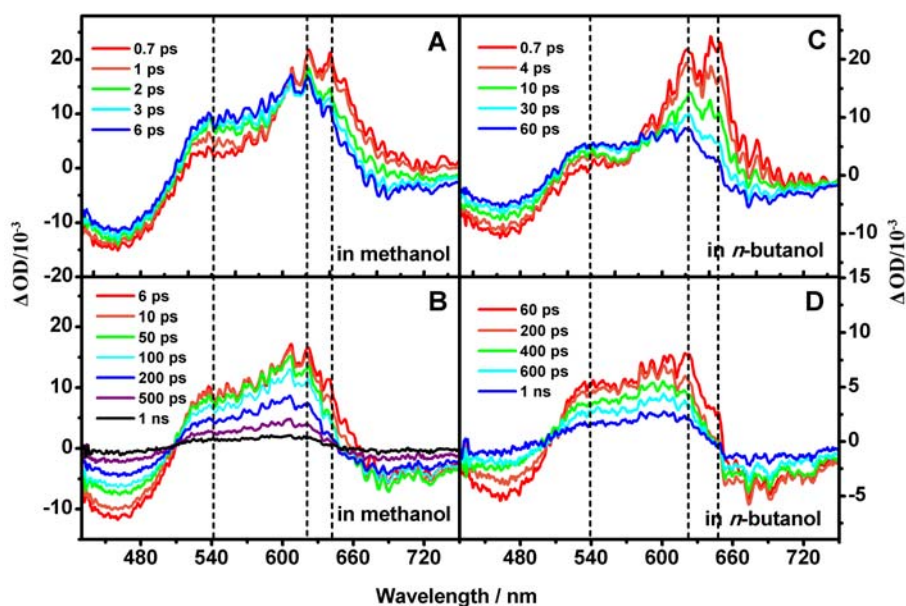

Figure S3. Evolution of the transient absorption spectra for NIAD-4 in methanol (A and B) and *n*-butanol (D and E) at different delay times.
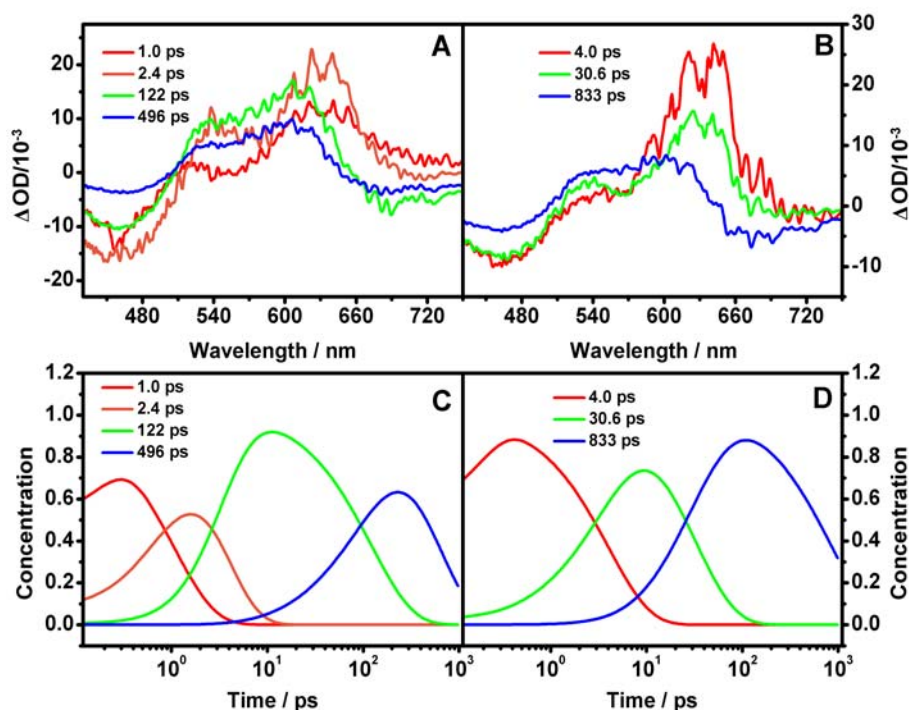
Figure S4. EADS from the global analysis for NIAD-4 in methanol (A) and *n*-butanol (B). Concentrations of the EADS components as a function of time in methanol (C) and *n*-butanol (D).

S4. Optimized geometries and the energy levels

Table S1 summarized five vertical excited state energies, oscillator strengths and orbital transitions with large coefficients of NIAD-4 in toluene. Table S2 summarized the optimized geometries of ground state (S_0), excited state (S_1) and two twisted intramolecular charge transfer state (TICT) of NIAD-4. The three dihedral angles (A1, A2 and A3) and the bond length for each optimized geometry were listed in Table S1. Bond length alternation values for all optimized geometry were presented in Table S1 as well. Figure S5 exhibits the energy of each optimized geometry both in ground state and excited state. The oscillator strength and energy difference were also labeled here. It is clear shows TICT state in the excited state whose oscillator strength is zero indicating that TICT state is a non-radiative. The planar S_1 state is an emission state which can be assign to ICT state considering the fact that the oscillator strength is nearly 1.

Table S1. Optimized geometries of ground state (S_0), excited state (S_1) and two twisted intramolecular charge transfer states (TICT) of NIAD-4.

	Optimized geometry	Dihedral angle			Bond length			Bond length alternation/ Å
		A1/°	A2/°	A3/°	A1/Å	A2/Å	A3/Å	
S_0		33.64	16.22	0.83	1.47	1.45	1.43	0.043

S$_1$ (ICT)		0.04	0.005	0.01	1.44	1.40	1.40	-0.010
TICT		20.74	2.13	85.22	1.45	1.40	1.43	0.004

Table S2. Five vertical excited state energies, oscillator strengths and orbital transitions with large coefficients of NIAD-4

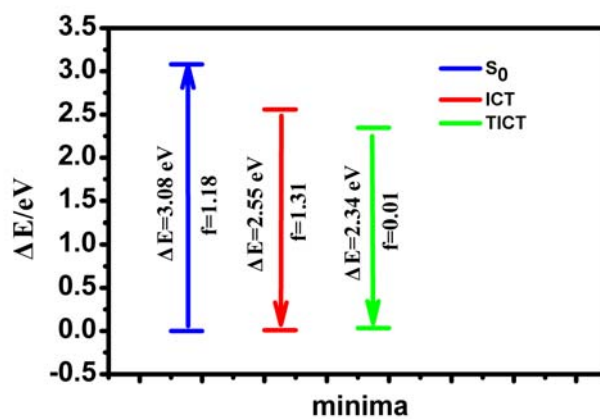|	Excited state energy (eV)	Oscillator strength	Orbital transition
S$_0$→S$_1$	2.8865	1.3460	HOMO→LUMO
S$_0$→S$_2$	4.1382	0.0351	HOMO-1→LUMO
S$_0$→S$_3$	4.4882	0.0602	HOMO-4→LUMO
S$_0$→S$_4$	4.5238	0.1059	HOMO→LUMO+1
S$_0$→S$_5$	4.6961	0.0264	HOMO-2→LUMO

Figure S5. The energy of each optimized geometry both in ground state and excited state (S$_0$, ICT, TICT) of NIAD-4 with the energy difference and oscillator strength of each transition.